

# Tunable Hybrid Photodetectors with Superhigh Responsivity\*\*

Song Liu, Jianfeng Ye, Yang Cao, Qian Shen, Zhongfan Liu,\* Limin Qi,\* and Xuefeng Guo\*

For practical applications, increasing the photosensitivity, response speed, and selectivity of UV photodetectors is a prerequisite.<sup>[1]</sup> Many research studies on Si-based photodiodes, the most common devices for UV detection, have been conducted to improve their photosensitivity.<sup>[1–3]</sup> The calculated photoresponsivities of these devices were typically less than  $10 \text{ A W}^{-1}$ .<sup>[4,5]</sup> Although these studies showed an improved performance, the devices exhibited some inherent limitations: the requirement for filters to block out visible and infrared photons, and the degradation of devices when exposed to UV light with energies much higher than the semiconductor bandgap.

With the obvious advantages of a room-temperature wide bandgap ( $E_g = 3.37 \text{ eV}$ ), low cost, and ease of manufacturing, zinc oxide (ZnO) is emerging as one of the most important materials for many applications in nanophotonics,<sup>[6]</sup> nanogenerators,<sup>[7–9]</sup> field-effect transistors (FETs),<sup>[10,11]</sup> sensors,<sup>[12]</sup> and so forth.<sup>[13,14]</sup> In particular, ZnO nanomaterials have recently been extensively investigated by several groups for UV photodetection applications.<sup>[15–28]</sup> For example, Soci et al.<sup>[15]</sup> reported ZnO nanowire photodetectors with a large photocurrent increase by several orders of magnitude upon UV illumination at a low light intensity. Lao et al.<sup>[16]</sup> successfully demonstrated the huge enhancement of the UV response of ZnO nanobelt sensors by close to five orders of magnitude after surface functionalization with a polymer that shows a high UV absorption ability. Zhang et al.<sup>[17]</sup> fabricated ZnO tetrapod-based sensors to distinguish false response and increase

sensitivity. These devices, however, were created using time-consuming nanowire growth and complex device fabrication. To improve the ability of large-area production, Jin et al.<sup>[20]</sup> nicely developed solution-processed UV photodetectors formed from thin films of colloidal ZnO nanoparticles but with a large cost to the responsivity (approximately  $61 \text{ A W}^{-1}$ ). By using high-quality ZnO epitaxial films grown on sapphire substrates, Liu et al.<sup>[28]</sup> fabricated Schottky UV photodetectors with a responsivity as high as  $400 \text{ A W}^{-1}$ . However, due to a lack of understanding of the structure–activity relationship and the presence of a large density of surface defects and grain boundaries, the UV responsivity of ZnO nanomaterials is limited.

Among the factors contributing to the high performance of the devices, we particularly pay attention to two main factors: the surface-to-volume ratio and the dimensionality of the materials. The large surface-to-volume ratio can greatly increase the number of surface trap states, thus prolonging the photocarrier lifetime. The reduced dimensionality can confine the active area of the charge carrier and therefore shorten the transit time. We expect that the combination of the large surface-to-volume ratio and the low dimensionality of the materials can lead to a high photoresponsivity of the devices. Herein, we demonstrate that a responsivity as high as five orders of magnitude can be achieved through surface functionalization of single-walled carbon nanotubes (SWNTs) as test-beds by using high-crystal-quality ZnO nanoparticles as antennas for UV detection (Figure 1). The ultrahigh responsivity in the devices is attributed to the synergistic effect of the high density of the surface trap states on the nanoparticle surface and the nature of the zero dimensionality of the nanoparticles. Another significant feature employed in this study is the use of the inherent ultrasensitivity of SWNT transistors arising from their

[\*] Prof. X. Guo, Prof. L. Qi, Prof. Z. Liu, S. Liu, J. Ye, Y. Cao, Q. Shen  
Center for Nanochemistry (CNC)  
Beijing National Laboratory for Molecular Sciences (BNLMS)  
State Key Laboratory for Structural Chemistry of Unstable and Stable Species  
College of Chemistry and Molecular Engineering  
Peking University  
Beijing 100871 (P. R. China)  
E-mail: guoxf@pku.edu.cn; liminqi@pku.edu.cn;  
zfliu@pku.edu.cn

[\*\*] We thank Yunqi Liu and Gui Yu for enlightening discussions. We acknowledge the financial support from FANEDD (No. 2007B21), MOST (2009CB623703, 2007CB936201), and NSFC (Grant Nos. 50873004, 20673007, 50821061, and 20833001).

Supporting Information is available on the WWW under <http://www.small-journal.com> or from the author.

DOI: 10.1002/sml.200900576

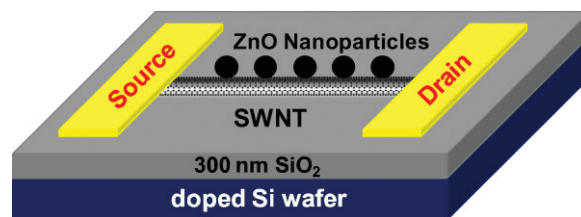


**Figure 1.** Schematic of SWNT transistors coated by ZnO nanoparticles. The ZnO nanoparticles are functionalized by dodecanoic acid, the alkane chains of which act as anchors to hold the nanoparticles close to the tube surface.

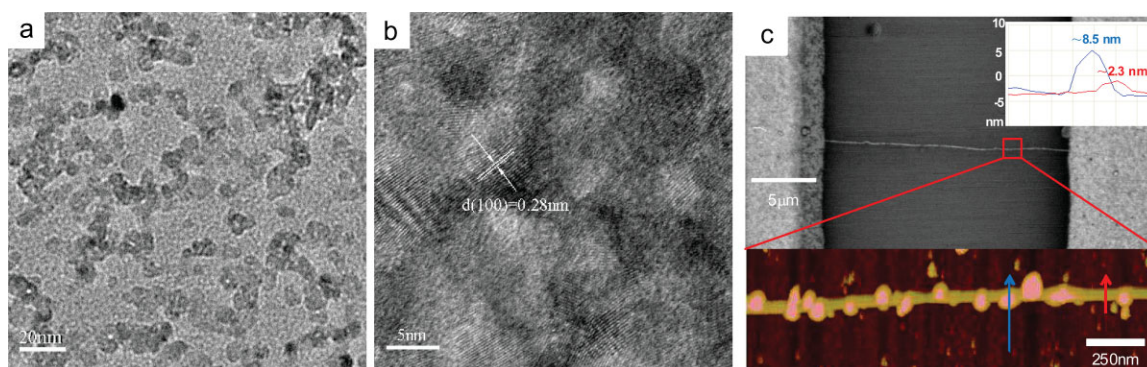


**Figure 2.** A) TEM and B) HRTEM images of ZnO nanoparticles. These highly crystalline monodisperse ZnO nanoparticles  $\sim 6$  nm in diameter are derivatized with dodecanoic acid. C) SEM and AFM images of a representative single tube on a silicon wafer assembled by ZnO nanoparticles. The tube is  $\sim 2.3$  nm in diameter. The average diameter of the ZnO nanoparticles is  $\sim 6$  nm. Inset: height profile across a nanoparticle and a tube, which indicates the height of the tube (red) and the nanoparticle (blue).

active surface being exposed to the environment, which has been utilized by us and other groups for the purpose of developing photosensitive SWNT-based FET devices.<sup>[29–40]</sup> Because ZnO nanoparticles show a different photosensitivity to light of different wavelengths, the resultant devices exhibit tunability of the conductance in devices by different UV light. These exciting findings could greatly speed up the application of ZnO nanomaterials for UV detection.

In our experiments, highly crystalline monodisperse ZnO nanoparticles about 6 nm in diameter were synthesized by the method detailed in the Experimental Section. The resulting ZnO nanoparticles were then derivatized with dodecanoic acid, because it has been demonstrated by us and others<sup>[30,31,34,36,37,41]</sup> that the long alkane chains of dodecanoic acids can noncovalently associate with the surface of carbon nanotubes and therefore act as anchors to hold the photoactive ZnO nanoparticles close to the tube surface. Figure 2A and B show transmission electron microscopy (TEM) and high-resolution TEM (HRTEM) images, respectively, of these highly crystalline monodisperse ZnO nanoparticles after functionalization with dodecanoic acid.

We next turn our attention to the preparation of SWNT transistors using our previous procedure.<sup>[29–31,42,43]</sup> In brief, individual SWNTs of high electrical quality were grown by a standard chemical vapor deposition (CVD) procedure from CoMo-doped mesoporous  $\text{SiO}_2$  catalyst nanoparticles by using ethanol as the carbon source. The catalyst particles were patterned on doped silicon wafers that had 300 nm of thermally grown  $\text{SiO}_2$  on their surface. Au (50 nm) on Cr (3 nm) leads, which are separated by 20  $\mu\text{m}$ , form the source and drain contacts to an individual SWNT through thermal evaporation. Figure 2C shows a representative scanning electron microscopy (SEM) image of an individual straight SWNT spanning source and drain electrodes on a silicon oxide surface. The highly doped silicon wafer serves as a global back-gate electrode for the devices. After initial electrical characterization and selection of individual semiconducting carbon-nanotube devices, ZnO nanoparticles were directly assembled on the surface of the pristine nanotubes by immersion of the devices into a dichloromethane solution ( $\approx 1.9 \text{ g L}^{-1}$ ) for 10 min. Then the devices were removed from the solution and rinsed with

fresh dichloromethane and acetone. Figure 2C also shows the high-resolution atomic force microscopy (AFM) image of the same tube, which indicates the successful assembly of ZnO nanoparticles on the tube surface.

In addition to the AFM technique, the successful attachment of ZnO nanoparticles on the tube surface can also be proved by the changes in the electrical characteristics of the devices. The electrical characteristics of the transistors were measured by applying a fixed source–drain bias voltage ( $V_{\text{sd}} = -5 \text{ mV}$ ) and sweeping the gate voltage ( $V_{\text{g}}$ ) between +9 and  $-9 \text{ V}$  in 0.15-V steps with an Agilent 4155C apparatus. We observed significant changes in the transfer characteristics of these transistors before and after self-assembly in the dark. Figure 3A illustrates the transfer characteristics for a semiconducting tube at each step of the process. To eliminate potential artifacts from gate hysteresis, we acquired all of the current–voltage ( $I$ – $V$ ) curves on the same measurement cycle while scanning from positive to negative bias. We observed very stable  $I$ – $V$  curves for a specific SWNT device under fixed experimental conditions, and thus they can be used to detect the photoswitching effect. Before self-assembly, this device indicates typical p-type semiconducting FET behavior with a threshold voltage ( $V_{\text{th}}$ ) at  $\sim 8.0 \text{ V}$ . Upon the assembly of the materials, we observed that  $V_{\text{th}}$  of this device shifted toward a negative value at  $\approx 6.8 \text{ V}$ , a clear change larger than 1 V, with a slight increase in the on-state resistance ( $R_{\text{on}}$ ). We also found that this shift in  $V_{\text{th}}$  is universal for SWNTs after assembly. These results are consistent with those of our control experiments. We measured the device characteristics when the devices were immersed in a dichloromethane solution of dodecanoic acid ( $\approx 1.0 \times 10^{-2} \text{ mol L}^{-1}$ ), removed, and rinsed with fresh dichloromethane and acetone as described above for ZnO nanoparticles. We observed similar shifts in  $V_{\text{th}}$  to those shown in Figure 3A. The  $I$ – $V$  curves can be found in the Supporting Information (Figure S1A). Given the  $V_{\text{th}}$  shifts, we infer that there should be a net negative charge transfer happening from dodecanoic acid to the nanotubes.<sup>[30,31,40]</sup> These results imply that dodecanoic acids have anchored to the surfaces of SWNTs. As a result, ZnO nanoparticles are adsorbed on the tube surfaces through dodecanoic acid anchors, as identified by the AFM image in Figure 2C.

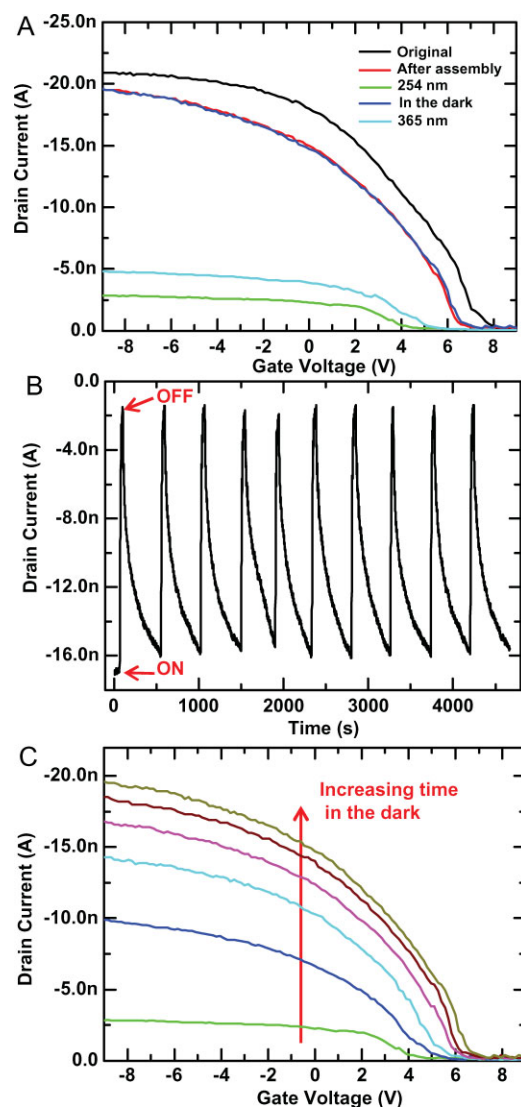


**Figure 3.** A) Changes in drain current of a p-type semiconducting device as a function of  $V_g$  before assembly (black), after assembly (red), under 254-nm UV irradiation for  $\sim 40$  s (green), under 365-nm UV irradiation for  $\sim 40$  s (cyan), and after UV light is off (blue). The source–drain bias voltage is held at  $-5$  mV. B) Time course of the drain current of the same device while 254-nm UV light is toggled on and off. The source–drain bias is  $-5$  mV; the gate bias is  $-2$  V. C) The gradual conversion from low- to high-conductance states when 254-nm UV light is removed. The current–voltage curves are taken every 80 s.

Once photoactive ZnO nanoparticles are coated on the tube surface, as expected, the device characteristics become very sensitive to UV light. We observed the very reversible and significant changes in  $R_{on}$  when the devices were measured under UV irradiation and in the dark. Figure 3A shows such a representative photoswitching effect in a device when a handheld UV lamp (254 nm, low intensity of  $\approx 26 \mu\text{W cm}^{-2}$ ) was switched on and off. Under UV irradiation at 254 nm, the initial high-conductance state (red curve in Figure 3A) turned into a low-conductance state (green curve) in a very short time. Moreover, the device recovered nearly to its original high-conductance state after the UV lamp was switched off (blue curve). We notice that  $V_{th}$  did not change obviously after a

whole photoswitching cycle, which implies that UV irradiation of ZnO nanoparticles could generate charge traps that affect the carrier scattering rate while the carrier concentration and Schottky barrier at the nanotube–electrode junction essentially remain unchanged during the process. Further experiments demonstrated that the photoswitching effect is a very reversible and fast process. Figure 3B shows the drain current as a function of time of the same device for a representative ten cycles while a  $-5$  mV source–drain bias and  $-2$  V gate bias were applied. After only a very brief UV irradiation (less than 40 s), the device decreased its drain current down to its low-conductance state. Figure 3C shows the gradual back-conversion from low- to high-conductance states when 254-nm UV light was removed. Remarkably, the switching process is reversible for at least 100 times without any degradation when UV light is toggled on and off. These photoswitching phenomena are quite reproducible, as we observed similar behavior on all of the functionalized semiconducting devices (over 15 devices).

To rule out potential artifacts, we performed control experiments. We examined the photoswitching effect of devices tethered only by dodecanoic acid anchors, that is, devices treated with dodecanoic acid but not with ZnO nanoparticles. The  $I$ – $V$  curves can be found in the Supporting Information (Figure S1B). There is only a slight increase in drain current under UV irradiation at 254 nm. It was reported that large opposite phenomena (current decrease) were observed in conventionally fabricated CVD-grown carbon-nanotube devices without any photoactive species under UV irradiation, mainly due to the Schottky barrier modulation caused by oxygen desorption.<sup>[44,45]</sup> In the present case, we used a much lower intensity of UV light ( $\approx 26 \mu\text{W cm}^{-2}$ ). More importantly, dodecanoic acids ( $\approx 1.0 \times 10^{-2} \text{ mol L}^{-1}$ ) in the high quantity used here on the nanotube surface cover the metal–nanotube junctions, thus precluding the possibility of oxygen desorption under UV illumination. As a result, we think that our dodecanoic acid-treated SWNT transistors show such a minimal current increase because of the intrinsic photoresponse of the tubes themselves under light irradiation.<sup>[46]</sup> In addition, a Schottky barrier formed at the junctions between the metal electrodes and the carbon nanotube could complicate the analysis during UV irradiation when the junctions are exposed to the photoactive nanoparticles. To preclude this possibility, we fabricated SWNT transistors with these junctions covered by an insulating layer (poly(methyl methacrylate), PMMA) that was patterned using electron-beam lithography. Then these junction-protected devices were treated by a hexane solution of ZnO nanoparticles. We observed essentially the same photoswitching effect as that shown in Figure 3. An optical micrograph of the device and the electrical characteristics can be found in the Supporting Information (Figure S2). These results clearly prove that the photoactivity of ZnO nanoparticles tethered on the surface of SWNTs is responsible for the changes in device characteristics,<sup>[30,31,34–40]</sup> rather than a local change at the metal–nanotube junctions and then Schottky barrier-height modulation.

Early studies<sup>[15–28]</sup> indicated that there are two mechanisms of ZnO photoresponse: photogeneration–recombination of electron–hole pairs and adsorption–photodesorption of oxygen

on the surface of the materials. In general, oxygen molecules are adsorbed onto ZnO surfaces by capturing free electrons from the n-type ZnO [ $O_2(g) + e^- \rightarrow O_2^-(ad)$ ]. Upon exposure to UV light with energies larger than the bandgap of the materials, the adsorbed oxygen will be photodesorbed by capturing the photogenerated holes from inside the materials [ $h^+ + O_2^-(ad) \rightarrow O_2(g)$ ]. The former process decreases the conductance of the materials by trapping the free carrier, while the latter process enhances the conductance by increasing the carrier concentration. As reported in the literature,<sup>[15–28]</sup> this mechanism can explain the observation of the persistent photocurrent of the materials. In the current case, because the power of 254-nm light we used from a handheld UV lamp is very low ( $\approx 26 \mu W cm^{-2}$ ), the photoresponse should be dominated by the oxygen adsorption–photodesorption mechanism (Figure 4). Upon illumination by 254-nm UV light, electron–hole pairs are generated. The holes migrate to the surface of ZnO nanoparticles and then discharge the negatively charged oxygen ions at the surface to photodesorb oxygen from the surface. This process results in an increase of the free-electron concentration of n-type ZnO semiconductors. Because the SWNTs we used in this study are p-type semiconducting, these free electrons produce scattering sites for the hole carriers flowing through the tubes. These active sites can scatter the hole carriers and therefore lower the conductance in the p-type semiconducting devices, which is opposite to the results reported previously<sup>[15–28]</sup> in which ZnO nanomaterials were directly used as the conducting materials. When UV light is removed, oxygen readsorbs on the nanoparticle surface, thus returning the device to its original high-conductance state (Figure 4). The readsorption process of oxygen is relatively slow, thus leading to the long recovery time of the devices. We also found that the conductance recovery process was much slower when the experiments were performed under a  $N_2$  atmosphere. Details of the comparison of the photoresponsive behaviors of a functionalized device under an oxygen-rich/deficient atmosphere can be found in the Supporting Information (Figure S3). This mechanism can fully explain the reversible photoswitching effect of ZnO nanoparticle-coated SWNT transistors as described above. Another possibility is that the photoinduced adsorption and desorption of oxygen from the nanoparticle surfaces induce the shift in  $V_{th}$ , thus leading to the same photoswitching effect. However, it is

difficult to distinguish between the two mechanisms since the effect might be a combination of both.

Remarkably, the calculated responsivity ( $R$ ) of the device is superhigh, approximately  $3.05 \times 10^5 A W^{-1}$  at an intensity ( $I_{ill}$ ) of  $26 \mu W cm^{-2}$  for 254-nm UV light, obtained by using the conventional model for the calculation:<sup>[47]</sup>

$$R = \frac{I_{ph}}{P_{ill}} = \frac{|I_1 - I_{dark}|}{P_{ill}} \quad (1)$$

$$P_{ill} = I_{ill} \cdot S = I_{ill} \cdot 4\pi \left(\frac{D}{2}\right)^2 \cdot \left(\frac{50\%L}{D}\right) = I_{ill}\pi DL/2 \quad (2)$$

where  $I_{ph}$  is the drain photocurrent,  $I_1$  is the drain current under illumination,  $I_{dark}$  is the drain current in the dark,  $P_{ill}$  is the incident illumination power on the channel of the device,  $I_{ill}$  is the light power intensity,  $S$  is the overall surface area of the ZnO nanoparticles,  $\pi$  is the circular constant,  $D$  is the diameter of the average ZnO nanoparticles, and  $L$  is the channel length of the device (assuming that the maximum coverage ratio of ZnO nanoparticles on the tube surface is  $\approx 50\%$  based on the AFM image in Figure 2C, after the imaging convolution of the AFM tip size is taken into account, and the average diameter of the nanoparticles is  $\approx 6$  nm.  $V_d = -5$  mV and  $V_g = -2$  V). To date, this responsivity value is the highest in comparison with conventional photodetectors (typically less than  $10 A W^{-1}$ )<sup>[4,5]</sup> and UV photodetectors formed from ZnO thin films.<sup>[17,20,28]</sup> In this study, we used high-quality-crystal ZnO nanoparticles as antennas. On the one hand, the very large surface-to-volume ratio of ZnO nanoparticles can increase the number of surface trap states and facilitate oxygen adsorption and desorption at the ZnO surface. On the other hand, the zero dimensionality of ZnO nanoparticles can confine the active area of charge carriers and therefore avoid the diffusion process.<sup>[15,17,20]</sup> We also note that, in addition to the large surface-to-volume ratio and low dimensionality of ZnO nanoparticles, the use of the inherent ultrasensitivity of SWNT transistors as test-beds, which results from their active surface that is exposed to the environment, plays an important role in device photosensitivity. The conclusion is that utilization of the synergistic effects of the inherent ultrasensitivity of SWNT transistors and the active photoresponsivity of ZnO nanoparticles affords a superhigh responsivity for the hybrid photodetectors.

To check the ability for intrinsic “visible-blind” detection of the devices, the hybrid photodetectors were also employed to detect light with different wavelengths generated by a 150 W Xe lamp source. Figure 5 shows the drain current as a function of time for the same device as that in Figure 3 when exposed to light of different wavelengths while a  $-5$  mV source–drain bias and a  $-2$  V gate bias were applied. We found that the devices show different photosensitivities to light with different wavelengths. As shown in Figures 3A and 5, the devices are the most sensitive

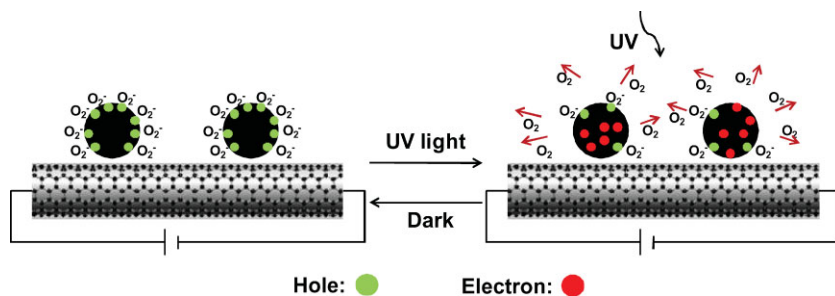


**Figure 4.** Illustration of how ZnO nanoparticles affect the device characteristics under UV irradiation and in the dark. To clearly demonstrate the mechanism, we removed dodecanoic acids at the surface of the ZnO nanoparticles, which are used to hold the nanoparticles close to the tube surface.

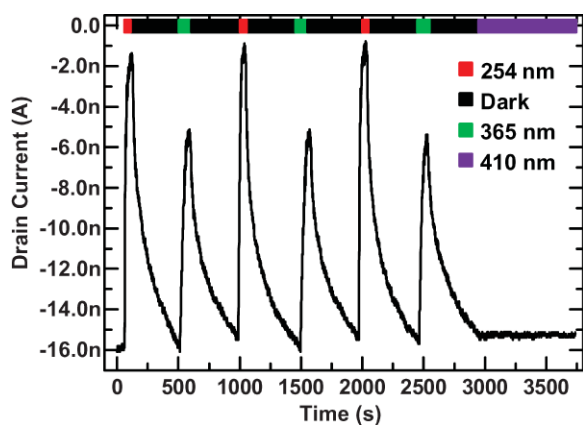


**Figure 5.** Illustration of the wavelength-dependent photoresponse of the same device as that in Figure 3 upon exposure to light of wavelength 254 (red), 365 (green), and 410 nm (purple) or in the dark (black).  $V_{sd} = -5$  mV and  $V_g = -2$  V.

to 254-nm light ( $\approx 26 \mu\text{W cm}^{-2}$ ) and less sensitive to 365-nm light ( $\approx 100 \mu\text{W cm}^{-2}$ ), but not to 410-nm light ( $\approx 100 \mu\text{W cm}^{-2}$ ). The calculated responsivity of the device to 365-nm UV light at an intensity of  $100 \mu\text{W cm}^{-2}$  is also very high, approximately  $5.83 \times 10^4 \text{ A W}^{-1}$  by the same method as that used above. The wavelength-dependent photosensitivity behavior of the devices is explained in detail below. The energy bandgap of the employed ZnO nanoparticles is  $\approx 3.37$  eV, which corresponds to light of wavelength  $\sim 369$  nm (see Figure S4, Supporting Information). This energy is smaller than that of light with wavelengths 254 ( $\approx 4.89$  eV) and 365 nm ( $\approx 3.40$  eV) but larger than that of light with wavelength 410 nm ( $\approx 3.03$  eV). As we all know, it is difficult to generate electron-hole pairs if the photon energy is smaller than the bandgap energy. This results in the hybrid devices being sensitive to the former two wavelengths but not to that of 410 nm. Because ZnO nanoparticles show different absorption intensities at different wavelengths (Figure S4, Supporting Information) and different photon energies are applied, it is reasonable that the devices exhibit a significant difference in photosensitivity to light at 254 and 365 nm. These results show a promising application of these hybrid photodetectors in the area of tunable light detection.

Finally, to prove the reliability and reproducibility of the photoswitching effect of the devices, we performed two control experiments for 365 nm as used for 254 nm. The  $I$ - $V$  curves of devices treated with dodecanoic acid but not with ZnO nanoparticles did not show any obvious changes in conductance upon illumination with 365-nm UV light (Figure S1C, Supporting Information). We also examined the photoswitching effect of the devices with the metal-SWNT junctions covered by an insulating layer of PMMA. We observed essentially the same photoswitching effect as that shown in Figure 3 (Figure S2, Supporting Information). These results strongly prove again that the photoactivity of ZnO nanoparticles tethered on the surface of SWNTs is responsible for the changes in device characteristics.

In summary, we have reported a method for fabricating tunable hybrid photodetectors with a responsivity as high as five orders of magnitude. The hybrid photodetectors are formed

from SWNT transistors as test-beds through surface functionalization of SWNTs by high-crystal-quality ZnO nanoparticles as antennas. The ultrahigh responsivity of the devices is attributed to the synergistic effects of the inherent ultrasensitivity of SWNT transistors and the active photoresponsivity of ZnO nanoparticles arising from the large surface-to-volume ratio and the nature of the zero dimensionality of the materials. Due to the photoinduced adsorption and desorption of oxygen from the nanoparticle surface, the resulting devices show significant photoswitching effects with good reversibility and reproducibility. Because ZnO nanoparticles show different photosensitivities to light of different wavelengths, the devices exhibit fine-tunability of the conductance in devices by different UV light. The concept used in this study, broadly applicable to a wide variety of low-dimensional nanomaterials, should have broad utility for making ultrasensitive devices for applications such as UV detection, sensing, imaging, optical communications, and memory storage.

## Experimental Section

**Synthesis of ZnO nanoparticles:** Zinc oxide nanoparticles with diameters of  $\sim 6$  nm were prepared according to the method reported in the literature.<sup>[11]</sup> Zinc acetate ( $\text{Zn}(\text{Ac})_2$ , 0.82 g, 4.46 mmol) and water (250  $\mu\text{L}$ ) were added to a flask containing methanol (42 mL). The solution was heated to  $60^\circ\text{C}$  with magnetic stirring. Potassium hydroxide (KOH, 0.49 g, 7.22 mmol, purity 85%) was dissolved in methanol (23 mL) as a stock solution that was added dropwise to the flask within 10–15 min. At a constant temperature of  $60^\circ\text{C}$ , it took 2.25 h to obtain 6-nm-diameter nanoparticles. The nanoparticles were separated from the solution (5 mL) obtained above by centrifugation, and washed with anhydrous ethanol three times. Then the precipitates were redispersed in an ethanol solution (10 mL) of dodecanoic acid ( $0.2 \text{ g L}^{-1}$ ). After reaction at room temperature for 2 h with magnetic stirring, the precipitates were collected by centrifugation. The dodecanoic acid-coated ZnO nanoparticles were easily dispersed in dichloromethane ( $1.9 \text{ g L}^{-1}$ ) for further application and characterization. TEM and HRTEM images were obtained on an FEI Tecnai F30 microscope operating at 300 kV.

**Device fabrication and characterization:** Ultralong individual SWNTs of high electrical quality were grown by a standard CVD procedure from CoMo-doped mesoporous  $\text{SiO}_2$  catalyst nanoparticles, by using ethanol as the carbon source on doped silicon wafers with 300 nm of thermally grown  $\text{SiO}_2$  on their surface.<sup>[30]</sup> Au (50 nm) on Cr (3 nm) leads, which were separated by  $20 \mu\text{m}$ , formed the source and drain contacts to an individual SWNT through standard thermal evaporation. The highly doped silicon wafer served as a global back-gate electrode for the devices. After initial characterization and selection of individual semiconducting carbon nanotube devices, ZnO nanoparticles were directly assembled on the surface of the pristine nanotubes by immersion of the devices in a dichloromethane solution ( $\approx 1.9 \text{ g L}^{-1}$ ) for 10 min. Then the devices were removed from the solution and completely rinsed with fresh dichloromethane and acetone. Junction-protected SWNT transistors insulated by PMMA were fabricated by electron-beam lithography. Then these devices were treated with a hexane solution of ZnO nanoparticles using

the method mentioned above. The devices were characterized with a standard probe station and semiconducting parameter analyzer (Agilent 4155C). Light irradiation was performed with 254-nm ( $\approx 26 \mu\text{W cm}^{-2}$ ) and 365-nm light ( $\approx 100 \mu\text{W cm}^{-2}$ ) generated by an 8 W handheld UV lamp, and with 410-nm light ( $\approx 100 \mu\text{W cm}^{-2}$ ) generated by a 150 W Xe lamp source. The power intensity of the light was measured by using an LPE-1A optical power meter (PhyScience Opto-Electronics Co., Ltd., Beijing) under the same experimental conditions. To avoid the heating effect during irradiation, the 410-nm light was focused and guided by a long optical fiber to the probe station.

### Keywords:

carbon nanotubes · nanoparticles · photosensitivity · UV detectors · zinc oxide

- [1] E. Monroy, F. Omnes, F. Calle, *Semicond. Sci. Technol.* **2003**, *18*, R33.
- [2] G. Dehlinger, S. J. Koester, J. D. Schaub, J. O. Chu, Q. C. Ouyang, A. Grill, *IEEE Photonics Technol. Lett.* **2004**, *16*, 2547.
- [3] Z. Pei, C. S. Liang, L. S. Lai, Y. T. Tseng, Y. M. Hsu, P. S. Chen, S. C. Lu, M. J. Tsai, C. W. Liu, *IEEE Electron Device Lett.* **2003**, *24*, 643.
- [4] K.-S. Lai, J.-C. Huang, K. Y. J. Hsu, *IEEE Trans. Electron Devices* **2008**, *55*, 774.
- [5] L. D. Garrett, J. Qi, C. L. Schow, J. C. Campbell, *IEEE Trans. Electron Devices* **1996**, *43*, 411.
- [6] Y. Nakayama, P. J. Pauzauskie, A. Radenovic, R. M. Onorato, R. J. Saykally, J. Liphardt, P. Yang, *Nature* **2007**, *447*, 1098.
- [7] X. Wang, J. Song, J. Liu, Z. L. Wang, *Science* **2007**, *316*, 102.
- [8] X. Wang, J. Zhou, J. Song, J. Liu, N. Xu, Z. L. Wang, *Nano Lett.* **2006**, *6*, 2768.
- [9] Z. L. Wang, J. Song, *Science* **2006**, *312*, 242.
- [10] J. Goldberger, D. J. Sirbully, M. Law, P. Yang, *J. Phys. Chem. B* **2005**, *109*, 9.
- [11] B. Sun, H. Siringhaus, *Nano Lett.* **2005**, *5*, 2408.
- [12] Z. L. Wang, *Annu. Rev. Phys. Chem.* **2004**, *55*, 159.
- [13] P. J. Pauzauskie, P. Yang, *Mater. Today* **2006**, *9*, 36.
- [14] C. M. Lieber, Z. L. Wang, *MRS Bull.* **2007**, *32*, 99.
- [15] C. Soci, A. Zhang, B. Xiang, S. A. Dayeh, D. P. R. Aplin, J. Park, X. Y. Bao, Y. H. Lo, D. Wang, *Nano Lett.* **2007**, *7*, 1003.
- [16] C. S. Lao, M.-C. Park, Q. Kuang, Y. Deng, A. K. Sood, D. L. Polla, Z. L. Wang, *J. Am. Chem. Soc.* **2007**, *129*, 12096.
- [17] Z. Zhang, L. Sun, Y. Zhao, Z. Liu, D. Liu, L. Cao, B. Zou, W. Zhou, C. Gu, S. Xie, *Nano Lett.* **2008**, *8*, 652.
- [18] J. H. He, Y. H. Lin, M. E. McConney, V. V. Tsukruk, Z. L. Wang, G. Bao, *J. Appl. Phys.* **2007**, *102*, 084303/1.
- [19] S. Mridha, D. Basak, *J. Appl. Phys.* **2007**, *101*, 083102/1.
- [20] Y. Jin, J. Wang, B. Sun, J. C. Blakesley, N. C. Greenham, *Nano Lett.* **2008**, *8*, 1649.
- [21] Y. Vygranenko, K. Wang, A. Nathan, *Appl. Phys. Lett.* **2006**, *89*, 172105/1.
- [22] J. Suehiro, N. Nakagawa, S.-i. Hidaka, M. Ueda, K. Imasaka, M. Higashihata, T. Okada, M. Hara, *Nanotechnology* **2006**, *17*, 2567.
- [23] C.-L. Hsu, S.-J. Chang, Y.-R. Lin, P.-C. Li, T.-S. Lin, S.-Y. Tsai, T.-H. Lu, I. C. Chen, *Chem. Phys. Lett.* **2005**, *416*, 75.
- [24] J. Y. Park, Y. S. Yun, Y. S. Hong, H. Oh, J.-J. Kim, S. S. Kim, *Appl. Phys. Lett.* **2005**, *87*, 123108/1.
- [25] S. Kumar, V. Gupta, K. Sreenivas, *Nanotechnology* **2005**, *16*, 1167.
- [26] H. S. Bae, S. Im, *Thin Solid Films* **2004**, *469-470*, 75.
- [27] H. Kind, H. Yan, B. Messer, M. Law, P. Yang, *Adv. Mater.* **2002**, *14*, 158.
- [28] Y. Liu, C. R. Gorla, S. Liang, N. Emanetoglu, Y. Lu, H. Shen, M. Wraback, *J. Elec. Mater.* **2000**, *29*, 69.
- [29] A. K. Feldman, M. L. Steigerwald, X. Guo, C. Nuckolls, *Acc. Chem. Res.* **2008**, *41*, 1731.
- [30] X. Guo, L. Huang, S. O'Brien, P. Kim, C. Nuckolls, *J. Am. Chem. Soc.* **2005**, *127*, 15045.
- [31] S. Liu, J. Li, Q. Shen, Y. Cao, G. Zhang, Z. Liu, M. L. Steigerwald, C. Nuckolls, D. Xu, X. Guo, *Angew. Chem. Int. Ed.* **2009**, *48*, 4759.
- [32] T. Someya, P. Kim, C. Nuckolls, *Appl. Phys. Lett.* **2003**, *82*, 2338.
- [33] T. Someya, J. Small, P. Kim, C. Nuckolls, J. T. Yardley, *Nano Lett.* **2003**, *3*, 877.
- [34] J. M. Simmons, I. In, V. E. Campbell, T. J. Mark, F. Leonard, P. Gopalan, M. A. Eriksson, *Phys. Rev. Lett.* **2007**, *98*, 086802/1.
- [35] F. Wang, H. Gu, T. M. Swager, *J. Am. Chem. Soc.* **2008**, *130*, 5392.
- [36] L. Hu, Y.-L. Zhao, K. Ryu, C. Zhou, J. F. Stoddart, G. Gruner, *Adv. Mater.* **2008**, *20*, 939.
- [37] Y.-L. Zhao, L. Hu, J. F. Stoddart, G. Gruner, *Adv. Mater.* **2008**, *20*, 1910.
- [38] E. Artukovic, M. Kaempgen, D. S. Hecht, S. Roth, G. Gruener, *Nano Lett.* **2005**, *5*, 757.
- [39] D. S. Hecht, R. J. A. Ramirez, M. Briman, E. Artukovic, K. S. Chichak, J. F. Stoddart, G. Gruener, *Nano Lett.* **2006**, *6*, 2031.
- [40] Y.-L. Zhao, L. Hu, G. Gruner, J. F. Stoddart, *J. Am. Chem. Soc.* **2008**, *130*, 16996.
- [41] R. J. Chen, S. Bangsaruntip, K. A. Drouvalakis, N. W. S. Kam, M. Shim, Y. Li, W. Kim, P. J. Utz, H. Dai, *Proc. Natl. Acad. Sci. USA* **2003**, *100*, 4984.
- [42] X. Guo, J. P. Small, J. E. Klare, Y. Wang, M. S. Purewal, I. W. Tam, B. H. Hong, R. Caldwell, L. Huang, S. O'Brien, J. Yan, R. Breslow, S. J. Wind, J. Hone, P. Kim, C. Nuckolls, *Science* **2006**, *311*, 356.
- [43] X. Guo, S. Xiao, M. Myers, Q. Miao, M. L. Steigerwald, C. Nuckolls, *Proc. Natl. Acad. Sci. USA* **2009**, *106*, 691.
- [44] R. J. Chen, N. R. Franklin, J. Kong, J. Cao, T. W. Tomblor, Y. Zhang, H. Dai, *Appl. Phys. Lett.* **2001**, *79*, 2258.
- [45] M. Shim, J. H. Back, T. Ozel, K.-W. Kwon, *Phys. Rev. B* **2005**, *71*, 205411/1.
- [46] M. Freitag, Y. Martin, J. A. Misewich, R. Martel, P. Avouris, *Nano Lett.* **2003**, *3*, 1067.
- [47] M. C. Hamilton, S. Martin, J. Kanicki, *IEEE Trans. Electron Devices* **2004**, *51*, 877.

Received: April 5, 2009  
Published online: August 7, 2009